

# Bayesian Framework Approach for Prognostic Studies in Electrolytic Capacitor under Thermal Overstress Conditions

Chetan S. Kulkarni<sup>1</sup>, José R. Celaya<sup>2</sup>, Kai Goebel<sup>3</sup>, and Gautam Biswas<sup>4</sup>

<sup>1,4</sup> Vanderbilt University, Nashville, TN, 37235, USA

*chetan.kulkarni@vanderbilt.edu*

*gautam.biswas@vanderbilt.edu*

<sup>2</sup> SGT Inc. NASA Ames Research Center, Moffett Field, CA, 94035, USA

*jose.r.celaya@nasa.gov*

<sup>3</sup> NASA Ames Research Center, Moffett Field, CA, 94035, USA

*kai.goebel@nasa.gov*

## ABSTRACT

Electrolytic capacitors are used in several applications ranging from power supplies for safety critical avionics equipment to power drivers for electro-mechanical actuators. Past experiences show that capacitors tend to degrade and fail faster when subjected to high electrical or thermal stress conditions during operations. This makes them good candidates for prognostics and health management. Model-based prognostics captures system knowledge in the form of physics-based models of components in order to obtain accurate predictions of end of life based on their current state of health and their anticipated future use and operational conditions. The focus of this paper is on deriving first principles degradation models for thermal stress conditions and implementing Bayesian framework for making remaining useful life predictions. Data collected from simultaneous experiments are used to validate the models. Our overall goal is to derive accurate models of capacitor degradation, and use them to remaining useful life in DC-DC converters.

## 1. INTRODUCTION

Avionics systems play a critical role in many aspects of aircraft flight control. As the system complexity and flight criticality of functions performed by these systems increases, the related consequences of in-flight malfunctions are bound to increase. This drives the need for Integrated Vehicle Health Management (IVHM) technologies for flight-critical avionics. Studying and analyzing the performance degradation of embedded electronics in the aircraft domain is abso-

lutely necessary to increase aircraft reliability, assure in-flight performance, and reduce maintenance costs, (J. R. Celaya, Wysocki, Vashchenko, Saha, & Goebel, 2010; Ferrell, 1999). In addition to this, an understanding of the behavior of deteriorated components is needed as well as the capability to anticipate failures and predict the remaining useful life (RUL) of the electronic systems.

An avionics system module consists of hardware (power supply, Global positioning system (GPS) receiver, Intertial measurement unit (IMU)) and software (GPS software, INAV - integrated navigation solution) components (Kulkarni, Biswas, Bharadwaj, & Kim, 2010). Switched-mode power supplies are widely used in DC-DC converters because of their high efficiency and compact size. Buck-boost DC-DC converter steps voltage levels up/down based on the application requirements, in which electrolytic capacitors and metal oxide semiconductor field effect transistor (MOSFET) switches are known to have the highest degradation and failure rates among all of the components (Goodman, 2005). Degraded capacitors affect the performance and efficiency of the DC-DC converters in a significant manner and also impose a risk on instantiating cascading failures on other connected subsystems.

In this paper we develop an effective prognostics and health management (PHM) methodology that applies to electronic systems and components. In particular, we develop a methodology to enable early detection of failure precursors in capacitor elements associated with DC-DC power supplies. Our approach combines physics-based modeling supported by empirical experimental analysis for improving the degradation models, and then implementing bayseain framework to predict remaining useful life of electrolytic capacitors. Our hy-

Chetan S. Kulkarni et al. This is an open-access article distributed under the terms of the Creative Commons Attribution 3.0 United States License, which permits unrestricted use, distribution, and reproduction in any medium, provided the original author and source are credited.

pothesis is that early detection will lead to better prediction and end of life estimates by tracking and modeling the degradation process.

The structure of the paper is as follows. Section II discusses the prognostics methodology implemented for this work. Section III presents introduction to electrolytic capacitors and its basic structure, operation and degradation mechanisms. Section IV discusses capacitor first principle models in detail. Section V describes the thermal stress aging experiments conducted for this work. Section VI and VII presents the prognostic framework methodology and RUL results respectively. The paper ends with discussion and conclusion in section VIII.

## 2. PROGNOSTIC METHODOLOGY

Prognostics is the process of predicting health condition and remaining useful life based on current and previous state, current and future operating conditions. Prognostics and health management (PHM) methods combine sensing, data collection, interpretation of environmental, operational, and performance related parameters to indicate systems health as well as anticipate damage propagation due to degradation. PHM methodologies can be implemented through the use of various techniques that study parameter variations, which indicate changes in performance degradation based on usage duration and conditions.

Prognostics is an essential technology for improving system safety, reliability, and availability. Prognostics deals with determining the health state of components, and projecting its health evolution into the future to make end of life (EOL) and remaining useful life (RUL) estimations. Model-based prognostics approaches perform these tasks with the help of first principles based physics models that capture knowledge about the system, its components, and their failures (Daigle & Goebel, 2011; Saha & Goebel, 2009).

We adopt an approach wherein we develop detailed physics-based models of components and systems that include descriptions of how fault parameters evolve in time. The implemented prognostics architecture is as shown in Figure 1. We have implemented this approach on empirical degradation models in our earlier work (J. Celaya et al., 2011a; Kulkarni et al., 2012). Experimental studies are being conducted and first principles based degradation models are being derived using the descriptions mentioned in (Kulkarni, Celaya, et al., 2011; J. Celaya et al., 2011a; Fife, 2006; MIL-C-62F, 2008). Identifying the failure precursors and developing accurate models of degradation/ failure has been the most difficult problem of our research goal. These models depend on known as well as unknown and possibly time-varying wear parameters. Early detection and analysis may lead to better prediction and end of life estimates of the capacitor by tracking and modeling the degradation process. Faults and degra-

dations appear as parameter value changes in the model, and this provides the mechanisms for tracking system behavior under degraded conditions (J. Celaya et al., 2011a, 2011b). The derived state space models are then implemented in a Bayesian framework for prognostics.

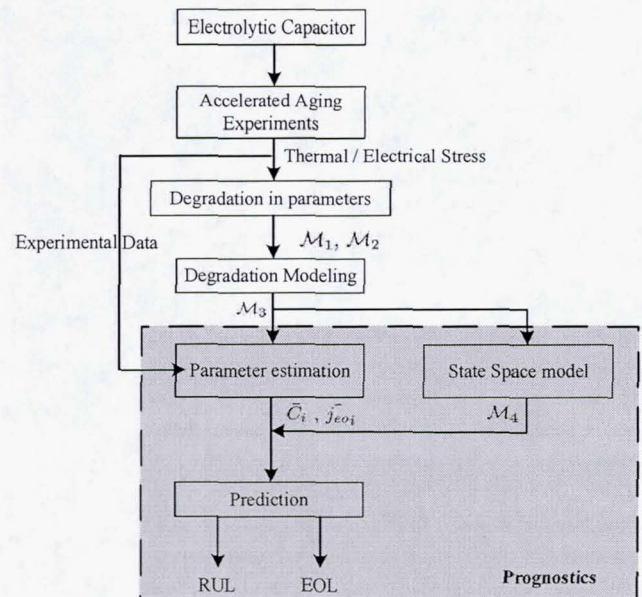


Figure 1. Prognostics Methodology

In the next section we discuss in brief the basics of electrolytic capacitors, their detailed structure and different mechanisms under which the devices degrade.

## 3. ELECTROLYTIC CAPACITORS

An aluminum electrolytic capacitor, as illustrated in Figure 2, consists of a cathode aluminum foil, electrolytic paper, electrolyte, and an aluminum oxide layer on the anode foil surface, which acts as the dielectric. When in contact with the electrolyte, the oxide layer possesses an excellent forward direction insulation property (Bengt, 1995). Figure 3 shows a

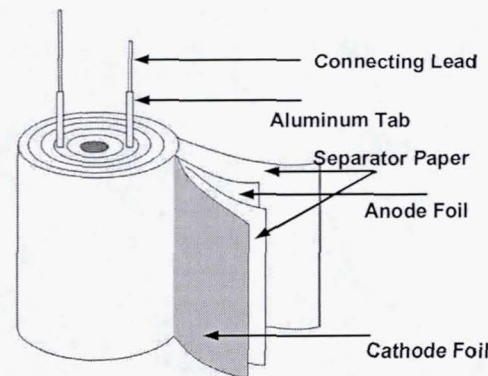


Figure 2. Illustration of an Electrolytic Capacitor

detailed view of the cross section of an electrolytic capacitor structure. To get higher capacitance values for the same surface area of the anode and cathode foils, the foil is etched by a chemical process. Together with magnified effective surface area attained by etching the foil, a high capacitance value is obtained in a small volume (Fife, 2006). Since the oxide layer has rectifying properties, a capacitor has polarity. If both the anode and cathode foils have an oxide layer, the capacitors would be bipolar. In this work, we analyze non-solid aluminum electrolytic capacitors in which the electrolytic paper is impregnated with liquid electrolyte. After etching, the plates are anodized by coating them with a thin aluminum oxide layer on the surface of the foil. This layer of aluminum oxide acts as the dielectric (insulator) and serves to block the flow of direct current between the two capacitor plates (Fife, 2006).

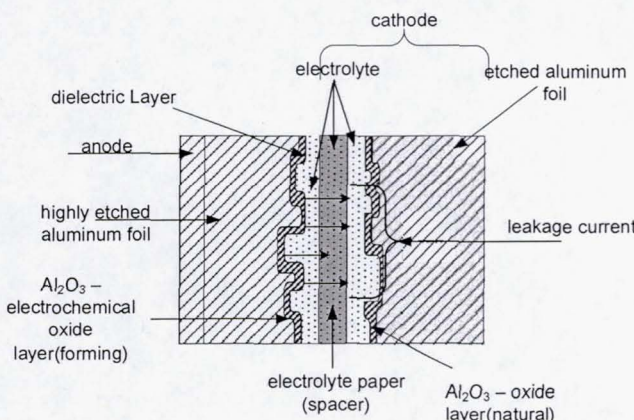


Figure 3. Capacitor Detail Structure

Electrolytic capacitor performance is strongly affected by its operating conditions, such as voltage, current, frequency, and ambient temperatures. Degradation in the capacitor manifests an increase in the equivalent series resistance (*ESR*) and decrease in capacitance (*C*), due to deterioration of electrolyte quality, decreases in electrolyte volume due to evaporation, weakening of the oxide layer, over operating time (Bengt, 1995; Fife, 2006). The *ESR* of a capacitor is the sum of the resistance due to aluminum oxide, electrolyte, spacer, and electrodes (foil, tabbing, leads, and ohmic contacts) (Bengt, 1995) and capacitance is the ability of a capacitor to store charge in an electric field. The health of a capacitor is often measured by the values of these two parameters.

There are certain industry standard thresholds for these parameter values, if the measurements exceed these thresholds then the component is considered unhealthy, i.e., the component has reached its end of life, and should be immediately replaced before further operations (Lahyani, Venet, Grellet, & Viverge, 1998). Failures in a capacitor can be one of two types: (1) catastrophic failures, where there is complete loss

of functionality due to a short or open circuit, and (2) degradation failures, where there is gradual deterioration of capacitor due to accumulated damages.

The fishbone diagram in Figure 6 summarizes the most common set of failure modes for electrolytic capacitors that have been discussed in (J. Celaya et al., 2011a; Kulkarni et al., 2012). This diagram identifies the relationship between root causes and failure modes observed in electrolytic capacitors. These root causes can occur individually or combined manner in a capacitor depending upon the conditions of operation. Our focus in this work is on the thermal stressors that govern the capacitor degradation, specifically, we study high temperature scenarios and their effects on the electrolytic capacitor degradation.

### 3.1. Equivalent Electrical Circuits

A simplified electrical lumped parameter model of impedance,  $\mathcal{M}_1$ , defined for an electrolytic capacitor is shown in Figure 4. The *ESR* dissipates some of the stored energy in the capacitor. An ideal capacitor would offer no resistance to the flow of current at its leads.

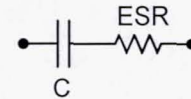


Figure 4. Lumped Parameter Model (  $\mathcal{M}_1$  )

It has been observed that under thermal overstress storage conditions (Bengt, 1995; J. Celaya et al., 2011a), the capacitance (*C*) and *ESR* value depends of the electrolyte resistance  $R_E$ . A more detailed lumped parameter model derived for an electrolytic capacitor under thermal overstress condition,  $\mathcal{M}_2$  can be modified from  $\mathcal{M}_1$ , as shown in Figure 5.  $R_1$  is the combined series and parallel resistances in the model.  $R_E$  is the electrolyte resistance. The combined resistance of  $R_1$  and  $R_E$  is the *ESR* of the capacitor. *C* is the total capacitance of the capacitor as discussed earlier.

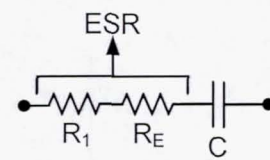


Figure 5. Lumped Parameter Model (  $\mathcal{M}_2$  )

## 4. PHYSICS BASED MODELING

In this section we discuss about deriving the first principles based degradation models for capacitors under thermal overstress conditions. Under thermal overstress conditions since the device was subjected to only high temperature with no charge applied we observe degradation only due to electrolyte

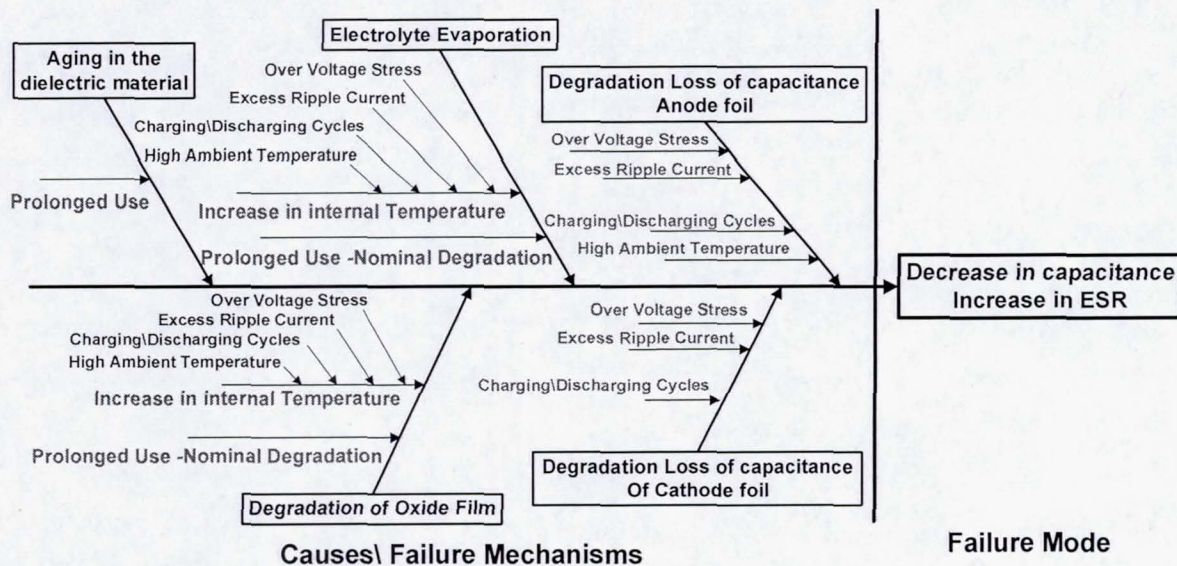


Figure 6. Fishbone diagram of failure mechanisms in aluminum electrolytic capacitor

evaporation. The degradation models are derived based on the underlying physics of operation and measurements from experimental data.

#### 4.1. Structural Model

For deriving the physics based models of an electrolytic capacitor it is also necessary to know about the structural and manufacturing details, since health estimations are done based on the type of electrolyte, volume of electrolyte, oxide layer thickness etc. The models defined use this information for making effective degradation/failure predictions. A detail structural study of the electrolytic capacitor under test is discussed in this section.

During modeling it is not possible to know the exact amount of electrolyte present in a capacitor. But using information from the structural details as shown in Figure 7, we can approximately calculate the amount of electrolyte present. A very highly porous separator paper is used which soaks all the electrolyte. The paper separator is sandwiched between anode and cathode, each having a thickness  $d_S$ ,  $d_A$  and  $d_C$  respectively ( $d_S \approx d_A \approx d_C$ ). Based on the type and configuration, the electrolyte volume will vary which can be updated in the model parameters.

The equation for calculating the approximate electrolyte volume is derived from calculating the total capacitor capsule volume,  $V_c$  given by :

$$V_c = \pi r_c^2 h_c \quad (1)$$

where :

$r_c$  = radius of capacitor capsule

$h_c$  = height of capacitor capsule

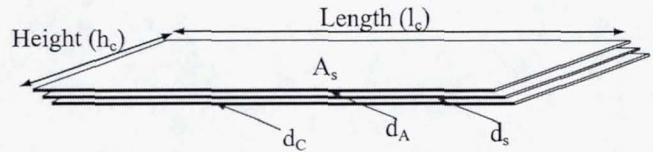


Figure 7. Capacitor open structure

The approximate electrolyte volume,  $V_e$  based on all the other known structural details of the capacitor can expressed as:

$$V_e = \pi r_c^2 h_c - A_s (d_A + d_C) \quad (2)$$

#### 4.2. Capacitance Degradation Model

Exposure to high temperatures,  $T_{applied} > T_{rated}$  results in accelerated aging of capacitors (Kulkarni, Celaya, et al., 2011; J. Celaya et al., 2011a; 60068-1, 1988). Higher ambient storage temperature accelerates the rate of electrolyte evaporation leading to degradation of the capacitance (Kulkarni, Celaya, et al., 2011; Bengt, 1995). The depletion in electrolyte volume,  $V_e$ , (Kulkarni, Biswas, et al., 2011; Rusdi et al., 2005) is given by :

$$V_e(t) = V_o - (A_s j_{eo} w_e) \times t \quad (3)$$

where:

$V_o$  = initial electrolyte volume

$j_{eo}$  = evaporation rate ( $\text{mg min}^{-1} \text{ area}^{-1}$ )

$w_e$  = volume of ethyl glycol molecule

$t$  = time in hours.

The total lumped capacitance from first principles of electro-

magnetism is given by :

$$C = (2\epsilon_R \epsilon_0 A_s) / d_C \quad (4)$$

where:

$\epsilon_R$  = relative dielectric constant

$\epsilon_0$  = permittivity of free space

Thus from Eq. (3) and Eq. (4) we can derive the first principles capacitance degradation model,  $\mathcal{M}_3$  given by :

$$\mathcal{M}_3 : C(t) = \left( \frac{2\epsilon_R \epsilon_0}{d_C} \right) \left( \frac{V_0 - V_e(t)}{j_{eo} t w_e} \right) \quad (5)$$

As discussed earlier, increase in the core temperature evaporates the electrolyte thus decreasing the electrolyte volume leading to degradation in capacitance. The resultant decrease in the capacitance can be computed using model,  $\mathcal{M}_3$  wherein the decrease in electrolyte volume, ( $V_e$ ) leads to decrease in capacitance, ( $C$ ).

### 4.3. Dynamic Models

The electrolyte volume,  $V_e$  can also be calculated and can also be expressed as  $V_e = A_s \cdot d_C$ . Hence the oxide surface area,  $A_s$  can be expressed in terms of electrolyte volume,  $V_e$  and oxide thickness,  $d_C$  as:

$$A_s = \frac{V_e}{d_C}. \quad (6)$$

From Eq. (4) and Eq. (6), dynamic capacitor degradation model can be updated as :

$$C_k = \left( \frac{2\epsilon_R \epsilon_0}{d_C} \right) \left( \frac{V_{e(k)}}{d_C} \right) \quad (7)$$

From Eq. (3) the first order discrete approximation for change in electrolyte volume can be expressed as:

$$\begin{aligned} \frac{dV_e}{dt} &= -(w_e A_s j_{eo}), \\ V_{e(k+1)} &= V_{e(k)} + \frac{dV_e}{dt} \Delta t, \\ V_{e(k+1)} &= V_{e(k)} - (w_e A_s j_{eo}) \Delta t. \end{aligned} \quad (8)$$

From Eq. (7) we have,

$$\begin{aligned} V_{e(k)} &= \frac{C_k}{2\epsilon_R \epsilon_0} d_C^2, \\ V_{e(k)} &= (C_k) \alpha. \end{aligned} \quad (9)$$

where:

$$\alpha = \frac{d_C^2}{2\epsilon_R \epsilon_0}$$

From Eq. (9) we can express Eq. (8) as :

$$\begin{aligned} C_{k+1} \alpha &= C_k \alpha + \frac{dC}{dt} \Delta t, \\ C_{k+1} \alpha &= C_k \alpha - (w_e A_s j_{eo}) \Delta t, \text{ hence} \\ C_{k+1} &= C_k - \frac{(w_e A_s j_{eo})}{\alpha} \Delta t. \end{aligned} \quad (10)$$

The complete discrete time dynamic model for capacitance degradation can be summarized as :

$$\mathcal{M}_4 : C_{k+1} = C_k - \frac{(2\epsilon_R \epsilon_0 w_e A_s j_{eo})}{d_C^2} \Delta t \quad (11)$$

Model  $\mathcal{M}_4$ , in Eq. (11) is implemented in a Bayesian tracking framework. In this work we are implementing a un-scented Kalman filter (UKF) since the degradation in capacitance (state) due to decrease in electrolyte is considered to be a dynamic linear model and the evaporation rate ( $j_{eo}$ ) parameter, assumed to be varying and estimated online. Next we discuss the implementation of the Bayesian framework methodology for prognostics (Saha & Goebel, 2009; Daigle et al., 2012; Daigle & Goebel, 2011).

### 5. UNSCENTED KALMAN FILTER

Estimation in nonlinear system is very important because many practical systems involve nonlinearities in their operation through one form or another. Estimation of the state accurately of such non-linear system is very important to diagnostics and be further implemented to prognostic applications which is extremely difficult. The Extended Kalman Filter (EKF) which applies the KF to nonlinear system by linearizing all nonlinear models, has become a most widely used method for estimation of nonlinear system. Although the EKF maintains is computationally efficient recursive update form of the KF for non-linear systems, it suffers a number of serious limitations (Julier & Uhlmann, 1997, 2004).

1. Only reliable if the error propagation to the future states can be approximated by a linear function.
2. Linearization can be applied only if the Jacobian matrix exists i.e, cannot be implemented if the system has discontinuities.
3. Calculating Jacobian matrices can be a very difficult and error-prone process.

The Unscented Kalman Filter (UKF) was proposed by (Julier & Uhlmann, 1997, 2004) to overcome these problems in non-linear systems. The unscented Kalman filter, instead of approximating the nonlinearity, approximates the state distribution (Julier & Uhlmann, 1997, 2004). This procedure maintains the nonlinear functions exactly, eliminating the need to calculate Jacobian's, and thereby providing an easier implementation framework. In this section we will look in the

detail framework of UKF which has been implemented for prognostics in this work.

A nonlinear system, described by the difference equation and the observation model with additive noise is given as :

$$\begin{aligned} x_k &= \mathbf{F}[x_{k-1}, u_{k-1}, k] + w_{k-1} \\ z_k &= \mathbf{H}[x_k, k] + v_k \end{aligned} \quad (12)$$

where  $x(k)$  is the  $n$ -dimensional state of the system at time step  $k$ ,  $u(k)$  is the input vector,  $w(k)$  is the process noise,  $Q$ ,  $z(k)$  is the observation vector and  $v_k$  is the measurement noise,  $R$ .

To solve the problem of predicting the future state or observation based on the Unscented transform (UT), UT takes a random variable  $x$ , with mean  $\bar{x}$  and covariance  $P_{xx}$ , which is related to a second random variable  $y$  by a nonlinear function  $y = f(x)$ . A small set of points (*sigma points*) with mean  $\bar{y}$  and covariance  $P_{yy}$  are selected (Julier & Uhlmann, 1997), which are deterministically selected and weighted to exhibit properties to match the mean and covarinace of the original distribution. A non-linear transformation is applied to each point to get the transformed points, statistics of the transformed points is then calculated to estimate the mean and covariance of the transformed points. The sigma point weights do not directly represent probabilities of the sigma points, and hence do not have to lie in the interval  $[0, 1]$ . The weights  $W_i$  can be positive or negative, but need to obey the following conditon to provide an unbiased estiamte.

$$\sum_i W_i = 1 \quad (13)$$

Each sigma point is instantiated through the function( $f$ ) to obtain new set of sigma points  $\mathcal{Y}$ .

$$\mathcal{Y}_i = f(\mathcal{X}_i) \quad (14)$$

The mean of the transformed points is given by:

$$\bar{y} = \sum_i W_i \mathcal{Y}_i \quad (15)$$

The covariance of the transformed points is given by:

$$P_{yy} = \sum_i W_i (x_o - \mu_0)(x_o - \mu_0)^T \quad (16)$$

The basic idea of the unscented transform is that it is easier to apporximate a probability distribution  $x$  than it is to approximate an arbitrary nonlinear function  $f$  or transformation (Julier & Uhlmann, 2004). This basic principle is implemented in the unscented Kalman filter where the unscented transform is exploited for nonlinear state estimation (Julier &

Uhlmann, 1997, 2004). At each step, the unscented transform is applied to the state estimate and is used for a single step prediction. In contrast, here, we apply the transform to the state parameter distribution at given single time point  $k_P$ , and use this for multi-step predictions to EOL. There are several methods which exits for selecting the sigma points out of which we implement the symmetric unscented transform for the prognosis problem (Daigle et al., 2012; Julier & Uhlmann, 2004). Detailed results will be presented in Section 6 for capacitor degradation problem.

In the symmetric unscented transform,  $2n_x + 1$  sigma points are selected symmetrically about the mean as follows (Julier & Uhlmann, 2004):

$$\begin{aligned} \mathcal{X}_0 &= \bar{x} \\ W_0 &= \frac{k}{n+k} \\ \mathcal{X}_i &= \bar{x} + \sqrt{((n+k)P_{xx})_i}, \\ W_i &= \frac{k}{2(n+k)} \\ \mathcal{X}_{i+n} &= \bar{x} - \sqrt{((n+k)P_{xx})_i} \\ W_{i+n} &= \frac{k}{2(n+k)} \end{aligned} \quad (17)$$

where  $\sqrt{((n+k)P_{xx})_i}$  refers to the  $i^{th}$  column of the matrix square root of  $(n+k)P_{xx}$ , computed using the Cholesky decomposition since it is numerically efficient and stable. Parameter  $k$  is used to tune the higher moments of distribution and suggested to have a smaller values as possible to bring the sigma points closer together. If  $x$  is assumed Gaussian, then selecting  $n+k = 3$  is recommended (Julier and Uhlmann, 1997).

## 6. THERMAL OVERSTRESS EXPERIMENT

In this setup we emulated conditions similar to high temperature storage conditions (Kulkarni, Celaya, et al., 2011; Kulkarni, Biswas, et al., 2011), where capacitors were placed in a controlled chamber and the temperature raised above their rated specification (60068-1, 1988). Pristine capacitors were taken from the same lot rated for 10V and maximum storage temperature rating of 85°C.

Experiments were conducted with 2200  $\mu\text{F}$  capacitors with TOS temperature at 105°C and humidity factor at 3.4%. The chamber temperature was gradually increased in steps of 25°C till the pre-determined temperature limit was reached. The capacitors were allowed to settle at a set temperature for 15 min and then the next step increase was applied. This process was continued till the required temperature limit was attained. To decrease possibility of shocks due to sudden de-

crease in the temperature the above procedure was followed. At the end of specific time interval the temperature was lowered in steps of  $25^{\circ}\text{C}$  till the required room temperature was reached.

Before being characterized the capacitors were kept at room temperature for 15 min. The ESR value is the real impedance measured through the terminal software of the instrument. Similarly the capacitance value is computed from the imaginary impedance using Electrochemical Impedance Spectroscopy (EIS). Characterization of all the capacitors was done for measuring the impedance values using an SP-150 Biologic impedance measurement instrument (Biologic, 2010). Figure 8 shows the plots decrease in capacitance due to accelerated aging for all the 15 capacitors under test at different aging times.

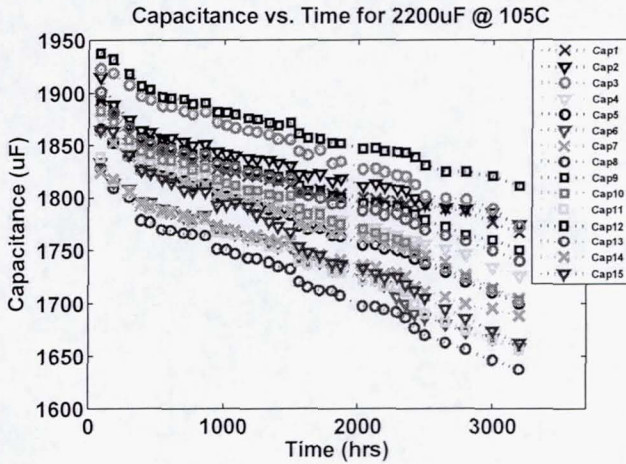


Figure 8. Capacitance Plot for all the devices under TOS

In the thermal overstress experiments, the capacitors we characterized periodically and after 3400 hours of operation it was observed that the average capacitance ( $C$ ) value decreased by more than 9-11% while decrease in  $ESR$  value was observed around 20 - 22%. From literature (60068-1, 1988) under thermal overstress conditions higher capacitance degradation is observed and minor degradation in  $ESR$  which correlated with the data collected. The failure thresholds under storage conditions for capacitance ( $C$ ) is 10% while that for  $ESR$  is around 280- 300% of the pristine condition values (60384-4-1, 2007; Kulkarni, Celaya, et al., 2011). Hence the capacitance degradation data was used as a precursor to failure parameter to estimate the current health condition of the device.

## 7. PREDICTION OF REMAINING USEFUL LIFE RESULTS

State estimation and RUL estimation results are discussed for capacitor Cap # 5 out of a batch of 15 available capacitors under test. Figure 9 shows the result of filter tracking for degradation in capacitance upto 3200 hours of aging time.

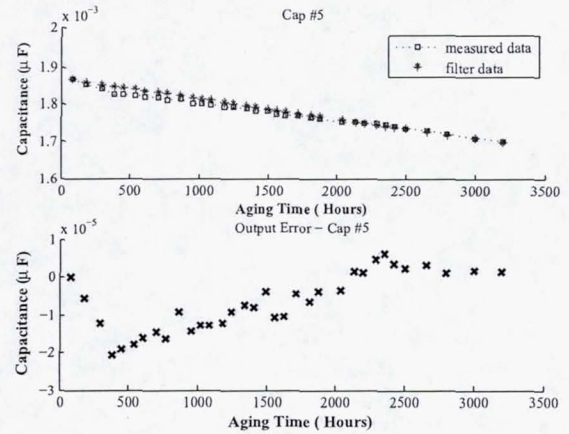


Figure 9. (a) Tracking filter output against measurement data, (b) Output error for Cap # 5

Figure 10 presents results from the remaining useful life prediction algorithm at different aging times  $t_p = 87, 607, 1495, 2131, 2800$  (hrs), at which the capacitors are characterized and their capacitance ( $C$ ) value is calculated. The failure threshold is considered to be 10% decrease in capacitance value, which in this case is at 3200 hours of aging time. End of life (EOL) is defined as the time at which the forecasted capacitance value trajectory crosses the EOL threshold. Therefore, RUL is EOL minus aging times  $t_p = 87, 607, 1495, 2131, 2800$  (hrs).

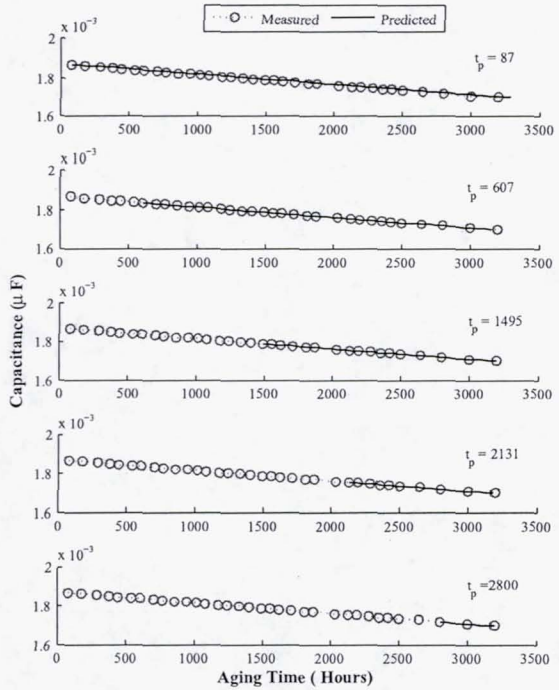


Figure 10. Capacitance decrease prediction at different Aging Time for Cap # 5

An  $\alpha$ - $\lambda$  prognostics performance metric (Saxena et al., 2009, 2008) is presented in Figure 11 for test case of Cap #5. The central dashed line represents ground truth and the shaded region is corresponding to a 30% ( $\alpha = 0.3$ ) error bound in the RUL prediction. Performance metric identifies whether the algorithm performs within desired error margins (specified by the parameter  $\alpha$ ) of the actual RUL at any given time instant (specified by the parameter  $\lambda$ ) (Saxena et al., 2009) and is based on relative accuracy (RA) metric in Eq. (18).

$$RA = 100 \left( 1 - \frac{RUL^* - RUL'}{RUL^*} \right) \quad (18)$$

Table 1 shows the performance summary based on the RA of all the capacitors under thermal stress performance. These metrics allows for an assessment of the percentage accuracy relative to the ground-truth value. RA values of 100 represent perfect accuracy. The RA is presented for all the test cases for different prediction times. The last column of Table 1 represents the median RA of all the test cases for a particular prediction time. It must be noted that if the prediction error magnitude grows beyond 100% RA gives a negative value. We do not consider such cases since these cases would not have qualify the tests for calculating RA (Saxena et al., 2009), these are indicated by NA in Table 1.

From the  $\alpha$ - $\lambda$  metric plot in Figure 11 it can be observed that the relative accuracy is not as good at the end but the accuracy is good enough under acceptable limits. This is due to the non-linearity observed in the data at the end of the aging time and the limitation of the model due to not including the oxide layer breakdown. The residuals show an increased error with aging time, since the breakdown in the oxide layer observed due to stress is not considered for this model which starts to dominate in the later stages of aging of the device. This breakdown is exponential in nature and as we can observe a dip in the capacitance values from the linear path in the later stages.

## 8. CONCLUSION AND DISCUSSION

This paper presents a first principles based degradation electrolytic capacitor model and an parameter estimation algorithm to validate the derived model, based on the experimental data. The majors contributions of the work presented in this paper are:

1. Development of the first principles degradation model based on accelerated life test aging data which includes decrease in capacitance as a function of time and evaporation rate linked to temperature conditions;
2. Implementation of a Bayesian based health state tracking and remaining useful life prediction (RUL) algorithm based on the UKF filtering framework;
3. Prediction of remaining useful life for capacitors based

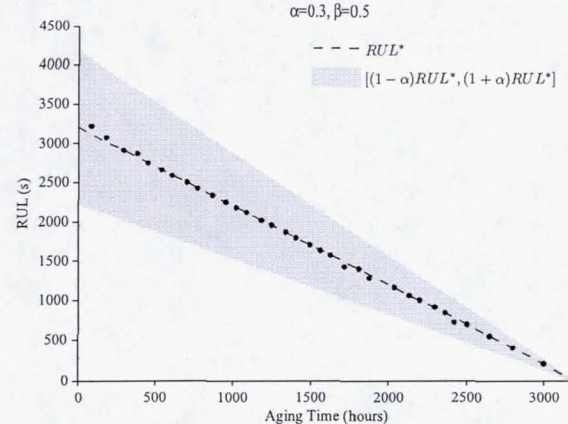


Figure 11. Performance based on Alpha-Lambda metric for Cap#5

first principles degradation model,  $\mathcal{M}_3$ :

The degradation model,  $\mathcal{M}_3$  based on the first principles gives an indication of how a specific device degrades based on its structure, material properties, operating conditions, etc. The results presented here are based on accelerated aging experimental data and on the accelerated life timescale. In our earlier work we studied the degradation models based on the observed data, and the work discussed here is a next step to generalize the model. Though as discussed in section 4, as a first step a dynamic linear model has been implemented for degradation model. This degradation model for decrease in capacitance,  $C$  and varying evaporation rate  $j_{eo}$  needs to be updated and include the model of break-down in the oxide layer which is exponential in nature and dominates in the later stages of aging. Further research will focus on development of functional mappings that will translate the accelerated life timescale into real usage conditions timescale, where the degradation process dynamics will be slower, and subjected to varying stress conditions.

The performance of the proposed first principles degradation model,  $\mathcal{M}_3$  is acceptable for the current study based on the quality of the model fit to the experimental data and the RUL prediction performance from  $\alpha$ - $\lambda$  metric plot. Additional experiments are currently underway to increase the number of test samples. This will greatly enhance the quality of the model, and guide the exploration of additional degradation models, where the loading conditions and the environmental conditions are also accounted for towards degradation dynamics.

## ACKNOWLEDGEMENT

Funding for this work was provided by PDM and VVFCS elements of the NASA/ARMD/Avsafe System-wide Safety and Assurance Technologies (SSAT) Project. Authors would also like to acknowledge Dr. Matthew J. Daigle and the members

of Prognostics Center of Excellence (PCoE) at NASA Ames Research Center for engaging in valuable and insightful discussions.

## NOMENCLATURE

$\epsilon_R$	relative dielectric constant
$\epsilon_0$	permittivity of free space
$V_o$	initial electrolyte volume
$j_{eo}$	evaporation rate ( $\text{mg min}^{-1} \text{ area}^{-1}$ )
$\rho_E$	electrolyte resistivity
$A_s$	effective oxide surface area
$w_e$	volume of ethyl glycol molecule
$d_A$	thickness of anode strip,
$d_C$	thickness of cathode strip
$d_s$	thickness of paper spacer
$M_1$	electrical lumped parameter model
$M_2$	updated lumped parameter model
$M_3$	capacitance degradation model
$M_4$	capacitance discrete time model

## REFERENCES

- 60068-1, I. (1988). Environmental testing, part 1: General and guidance. *IEC Standards*.
- 60384-4-1, I. (2007). Fixed capacitors for use in electronic equipment. *IEC Standards*.
- Bengt, A. (1995). Electrolytic capacitors theory and applications. *RIFA Electrolytic Capacitors*.
- Biologic. (2010). Application note 14-zfit and equivalent electrical circuits [Computer software manual].
- Celaya, J., Kulkarni, C., Biswas, G., & Goebel, K. (2011a). A model-based prognostics methodology for electrolytic capacitors based on electrical overstress accelerated aging. *Proceedings of Annual Conference of the PHM Society, September 25-29, Montreal, Canada*.
- Celaya, J., Kulkarni, C., Biswas, G., & Goebel, K. (2011b). Towards prognostic of electrolytic capacitors. *American Institute of Aeronautics and Astronautics, AIAA Infotech@Aerospace 2011, March 2011, St. Louis, Missouri*.
- Celaya, J. R., Wysocki, P., Vashchenko, V., Saha, S., & Goebel, K. (2010). Accelerated aging system for prognostics of power semiconductor devices. In *Ieee autotestcon, 2010* (p. 1-6). Orlando, FL.
- Daigle, M., & Goebel, K. (2011, March). Multiple damage progression paths in model-based prognostics. *Proceedings of the 2011 IEEE Aerospace Conference*.
- Daigle, M., Saha, B., & Goebel, K. (2012, March). A comparison of filter-based approaches for model-based prognostics. In *Proceedings of the 2012 ieee aerospace conference*.
- Ferrell, B. L. (1999). JSF prognostics and health management. *IEEE Aerospace Conference*, 471.
- Fife, J. (2006, August). *Wet electrolytic capacitors* (Patent No: 7,099 No. 1). Myrtle Beach, SC: AVX Corporation.
- Goodman, D. (2005, March). Practical application of phm/prognostics to cots power converters. *Aerospace Conference, 2005 IEEE*, 3573-3578.
- Julier, S. J., & Uhlmann, J. K. (1997). A new extension of the kalman filter to nonlinear systems. *Proceedings of the 11th International Symposium on Aerospace/Defense Sensing, Simulation and Controls*, 182 - 193.
- Julier, S. J., & Uhlmann, J. K. (2004). Unscented filtering and nonlinear estimation. *Proceedings of the IEEE*, 92(3), 401 - 422.
- Kulkarni, C., Biswas, G., Bharadwaj, R., & Kim, K. (2010, April). Effects of degradation in dc-dc converters on avionics systems: A model based approach. *Proceedings of the Machinery Failure Prevention Technology Conference (MFPT)*, 8-13.
- Kulkarni, C., Biswas, G., Celaya, J., & Goebel, K. (2011). A case study for capacitor prognostics under accelerated degradation. *IEEE 2011 Workshop on Accelerated Stress Testing & Reliability (ASTR), September 28-30, San Francisco, CA*.
- Kulkarni, C., Celaya, J., Biswas, G., & Goebel, K. (2011). Prognostic modeling and experimental techniques for electrolytic capacitor health monitoring. *The 8th International Workshop on Structural Health Monitoring 2011 (IWSHM), September 13-15, Stanford University, Stanford, CA*.
- Kulkarni, C., Celaya, J., Biswas, G., & Goebel, K. (2012). Prognostic and experimental techniques for electrolytic capacitor health monitoring. *The Annual Reliability and Maintainability Symposium (RAMS), January 23-36, Reno, Nevada..*
- Lahyani, A., Venet, P., Grellet, G., & Viverge, P. (1998, Nov). Failure prediction of electrolytic capacitors during operation of a switchmode power supply. *IEEE Transactions on Power Electronics*, 13, 1199-1207.
- MIL-C-62F. (2008). General specification for capacitors. *Fixed Electrolytic*.
- Rusdi, M., Moroi, Y., Nakahara, H., & Shibata, O. (2005). Evaporation from water ethylene glycol liquid mixture. *Langmuir - American Chemical Society*, 21 (16), 7308 - 7310.
- Saha, B., & Goebel, K. (2009, September). Modeling li-ion battery capacity depletion in a particle filtering framework. In *Proceedings of the annual conference of the prognostics and health management society 2009*.
- Saxena, A., Celaya, J., Balaban, E., Goebel, K., Saha, B., Saha, S., & Schwabacher, M. (2008). Metrics for evaluating performance of prognostic techniques. In *International conference on prognostics and health management 2008*.
- Saxena, A., Celaya, J., Saha, B., Saha, S., & Goebel, K.

(2009, September). On applying the prognostic performance metrics. In *Annual conference of the prognostics and health management society*.

**Chetan S. Kulkarni** is a Research Assistant at ISIS, Vanderbilt University. He received the M.S. degree in EECS from Vanderbilt University, Nashville, TN, in 2009, where he is currently a Ph.D candidate and received a B. E. degree in Electronics and Electrical Engineering from University of Pune, India in 2002.

**José R. Celaya** is a research scientist with SGT Inc. at the Prognostics Center of Excellence, NASA Ames Research Center. He received a Ph.D. degree in Decision Sciences and Engineering Systems in 2008, a M. E. degree in Operations Research and Statistics in 2008, a M. S. degree in Electrical Engineering in 2003, all from Rensselaer Polytechnic Institute, Troy New York; and a B. S. in Cybernetics Engineering in 2001 from CETYS University, México.

**Kai Goebel** received the degree of Diplom-Ingenieur from the Technische Universität München, Germany in 1990. He received the M.S. and Ph.D. from the University of California at Berkeley in 1993 and 1996, respectively. Dr. Goebel is a senior scientist at NASA Ames Research Center where he leads the Diagnostics and Prognostics groups in the Intelligent Systems division. In addition, he directs the Prognostics Center of Excellence and he is the technical lead for Prognostics and Decision Making of NASA's System-wide Safety and Assurance Technologies Program. He worked at General Electric's Corporate Research Center in Niskayuna, NY from 1997 to 2006 as a senior research scientist. He has carried out applied research in the areas of artificial intelligence, soft computing, and information fusion. His research interest lies in advancing these techniques for real time monitoring, diagnostics, and prognostics. He holds 15 patents and has published more than 200 papers in the area of systems health management.

**Gautam Biswas** received the Ph.D. degree in computer science from Michigan State University, East Lansing. He is a Professor of Computer Science and Computer Engineering in the Department of Electrical Engineering and Computer Science, Vanderbilt University, Nashville, TN.

Aging Time	C1	C2	C3	C4	C5	C6	C7	C8	C9	C10	C11	C12	C13	C14	C15	$\bar{RA}_a$
181.67	98.34	95.03	100.00	98.34	98.34	98.34	98.34	93.37	98.34	96.69	91.72	91.72	98.34	98.34	96.69	96.80
295.38	98.28	94.84	98.28	100.00	100.00	98.28	98.28	93.11	98.28	96.56	93.11	91.39	98.28	100.00	96.56	97.02
384.47	98.22	94.67	100.00	100.00	98.22	98.22	98.22	92.90	98.22	96.45	91.12	91.12	98.22	98.22	96.45	96.69
450.93	98.18	94.54	98.18	100.00	100.00	100.00	98.18	92.72	98.18	96.36	92.72	90.91	98.18	100.00	98.18	97.09
540.77	98.12	94.36	100.00	100.00	100.00	98.12	98.12	92.48	98.12	96.24	92.48	90.60	98.12	100.00	96.24	96.87
607.07	98.07	94.22	98.07	100.00	100.00	100.00	98.07	92.29	98.07	96.14	92.29	90.36	98.07	100.00	98.07	96.91
701.62	98.00	94.00	98.00	100.00	100.00	100.00	98.00	91.99	98.00	96.00	91.99	89.99	98.00	100.00	98.00	96.80
766.83	97.95	91.78	97.95	100.00	100.00	100.00	100.00	93.84	97.95	93.84	91.78	89.73	97.95	100.00	97.95	96.71
860.43	97.86	93.59	97.86	100.00	100.00	100.00	97.86	93.59	97.86	95.73	91.45	89.31	97.86	100.00	97.86	96.72
950.07	97.78	93.33	97.78	100.00	100.00	100.00	97.78	93.33	97.78	95.56	91.11	88.89	97.78	100.00	97.78	96.59
1019	100.00	90.83	97.71	100.00	100.00	100.00	100.00	93.12	97.71	93.12	93.12	88.54	95.41	100.00	97.71	96.48
1084.47	97.64	92.91	100.00	100.00	100.00	97.64	92.91	97.64	95.27	90.55	90.55	97.64	100.00	97.64	96.69	
1179.5	97.53	92.58	100.00	100.00	100.00	97.53	92.58	97.53	95.05	90.10	90.10	97.53	100.00	97.53	96.54	
1244.82	97.44	92.33	100.00	100.00	100.00	97.44	92.33	97.44	94.89	92.33	89.77	97.44	100.00	97.44	96.59	
1338.18	97.31	91.94	100.00	100.00	100.00	97.31	94.63	97.31	94.63	91.94	89.26	97.31	100.00	97.31	96.60	
1404.48	97.22	91.65	100.00	100.00	100.00	97.22	100.00	94.43	97.22	94.43	91.65	88.86	97.22	100.00	97.22	96.47
1495.4	97.07	91.20	100.00	100.00	100.00	97.07	97.07	94.13	97.07	94.13	91.20	88.27	97.07	100.00	97.07	96.09
1560.48	96.95	90.85	100.00	100.00	100.00	96.95	100.00	96.95	96.95	90.85	93.90	87.80	96.95	96.95	100.00	96.34
1626.53	96.82	93.64	96.82	100.00	100.00	96.82	96.82	96.82	100.00	93.64	90.47	90.47	96.82	100.00	96.82	96.40
1716.57	96.63	89.89	100.00	100.00	96.63	93.26	100.00	100.00	96.63	89.89	93.26	86.52	96.63	96.63	100.00	95.73
1807.02	96.41	89.23	96.41	100.00	100.00	92.82	100.00	100.00	96.41	92.82	96.41	89.23	96.41	96.41	100.00	96.17
1871.62	96.24	88.71	96.24	100.00	96.24	92.47	100.00	96.24	96.24	88.71	96.24	88.71	96.24	96.24	96.24	94.98
2036.88	91.40	91.40	91.40	100.00	100.00	91.40	95.70	95.70	100.00	91.40	95.70	91.40	100.00	95.70	100.00	95.41
2131.35	90.64	95.32	90.64	95.32	100.00	90.64	95.32	95.32	95.32	90.64	95.32	90.64	100.00	95.32	95.32	94.39
2196.1	90.04	95.02	90.04	100.00	100.00	90.04	95.02	90.04	95.02	90.04	100.00	95.02	100.00	95.02	95.02	94.69
2290.12	83.51	94.50	83.51	94.50	100.00	89.01	94.50	83.51	94.50	89.01	100.00	94.50	100.00	94.50	94.50	92.67
2355.97	82.23	94.08	82.23	94.08	100.00	82.23	94.08	82.23	94.08	88.15	100.00	100.00	100.00	94.08	88.15	91.71
2421.92	80.72	100.00	80.72	100.00	93.57	74.30	100.00	74.30	93.57	87.15	93.57	100.00	100.00	87.15	87.15	90.15
2500	71.43	100.00	71.43	92.86	100.00	71.43	92.86	64.29	85.71	85.71	92.86	92.86	85.71	85.71	85.71	
2650	54.55	90.91	54.55	90.91	100.00	63.64	90.91	54.55	72.73	90.91	81.82	81.82	90.91	81.82	72.73	78.18
2800	37.50	75.00	37.50	75.00	100.00	37.50	87.50	25.00	62.50	87.50	75.00	62.50	75.00	75.00	62.50	65.00
3000	NA	25.00	NA	50.00	100.00	0.00	75.00	NA	0.00	75.00	25.00	NA	50.00	50.00	25.00	43.18
$\bar{RA}_b$	87.13	90.78	87.99	96.60	99.39	89.29	94.45	85.73	92.14	92.50	90.32	87.15	95.49	94.97	92.38	

Table 1. Summary of RUL forecasting results

 $\bar{RA}_a$  is the mean relative accuracy of all capacitors at each prediction time ( $t_p$ ) $\bar{RA}_b$  is the mean relative accuracy of each capacitor at all prediction times